Hindawi
Advances in Civil Engineering
Volume 2018, Article ID 7876908, 10 pages
https://doi.org/10.1155/2018/7876908

Research Article

Seismic Behavior of Three-Story Prestressed Fabricated Concrete Frame under Dynamic and Low Reversed Cyclic Loading

Manrong Song[1], **Jiaxuan He**[1], **Yuan Liu**[1], **Hang Zhang**[2,3], **Chenjun Ge**[1], **Yadong Jin**[1], **Bingkang Liu**[1], **Shenjiang Huang**[1] and **Yan Liu**[4]

[1]*School of Civil Engineering, Hefei University of Technology, Hefei 230009, China*
[2]*School of Transportation, Wuhan University of Technology, Wuhan 430063, China*
[3]*Hubei Highway Engineering Research Center, Wuhan 430070, China*
[4]*State Key Laboratory of Explosion Science and Technology, Beijing Institute of Technology, Beijing 100081, China*

Correspondence should be addressed to Manrong Song; fgmsong@163.com and Shenjiang Huang; huangsj000@hotmail.com

Received 25 April 2018; Accepted 17 July 2018; Published 10 September 2018

Academic Editor: Hang Lin

Precast concrete structure is the building industrialization of the sure route. It can realize the construction process of low energy consumption and low emission and effectively meet the green development requirements of the construction industry. Based on prestressing technique, the connections of the precast concrete structure obtain prestress producing integrate joints and continuous frames, which improve the seismic safety and are applied widely in the earthquake area. To study seismic behavior of prestressed fabricated concrete frame structure, the experiments on the concrete frame under dynamic loading and low reversed cyclic loading were carried out. The single-span three-story prestressed fabricated concrete frame can accurately represent the load-carrying capability and the failure mechanism of multistory frame. Results of the study show that experimental specimens have good behaviors such as full hysteresis curves, proper displacement restoring capacity, and energy dissipation; the maximum interlayer drift ratio arrives 0.27% which has no damage to the frame in small earthquakes subjected to the 102 gal peak ground acceleration; the frame is repairable in moderate earthquakes when the maximal interlayer drift ratio arrives 0.73% subjected to the 204 gal peak ground acceleration; plastic hinges appeared at the ends of beam under low reversed cyclic loading firstly where the section curvature ductility factor ranges from 3.64 to 5.62; biaxial compression is acquired at beam-column joints with the help of column axial force and horizontal prestressing force; the beam fails before the column in the prestressed fabricated concrete frame at interlayer drift ratio between 1.56% and 2.56%.

1. Introduction

Precast concrete structure was originated from Western Europe and developed in Europe and North America. It has become a major architectural structure in the developed countries such as Europe, America, and Japan. With the perfection of precast concrete construction technology and the development of precast concrete structure system, precast concrete structure has the advantages of lower costs, faster construction, and improved quality, which is superior to the cast-in-situ concrete structure. Because the connections cannot satisfy the requirement of carrying capacity under seismic loading, precast concrete structure is supposed to be unreliable in earthquake-prone areas and has difficulty to generalize. In recent years, precast concrete structure has received more attentions, which has been known as the goal of building industrialization. Post-tensioning method has been employed in numerous seismic force-resisting systems as the pivotal technology of the restoring force mechanism that eliminates residual building drifts following seismic loading [1]. Based on posttensioning method, the connections of precast fabricated concrete structure obtain prestress producing integrate joints and continuous frame. The strands were passed through the reserved prestressed tendon ducts in beams and column, and then, they were stretched to form the integrated

beam-column connections. It is not only served as a kind of assembling means in the construction phase, but also bears the end moment of beam that the connections could transfer the moment at the end of beam effectively. Since the middle of 1990s, seismic design of precast structures has mainly relied on utilizing unbounded posttensioning to establish the connection between a precast member and an adjacent precast or cast-in-place concrete element [2–4]. The concept enables the precast fabricated concrete structure to experience minimum structural damage and offer self-centering capability when subjected to lateral forces.

The unbounded posttensioned precast concrete system was studied in America in the early time. A number of relevant experiments and theoretical analyses have been done on the connection configuration and performance of jointed concrete systems. Aaleti and Sritharan [5] studied unbounded posttensioned precast wall systems, single walls, and jointed wall systems designed with unbounded posttensioning experienced minimum structural damage and 2% drift under large lateral seismic loads, and were supposed to improve ductility and energy dissipation capacity. In order to evaluate the seismic performance of semirigid joint in multilayer precast frame, Haluk Sucuoglu calculated the inelastic seismic responses of precast concrete structures [6]. In the process of analysis, the fixity factors of precast concrete connections were used as variables. The analysis shows that when the fixity factors of the semirigid joint of precast concrete structure are greater than 0.8, there is little difference between the seismic response of precast structure and cast-in-place structure.

In 2003, European Community initiated the international cooperation program, European 5th Framework Program: *Seismic Behavior of Precast Concrete Structures with Respect to Eurocode 8*, aimed to investigate seismic behavior of the precast fabricated concrete structures and to modify Eurocode 8. Giandomenico Toniolo and Antonella Colombo examined the problems of precast concrete building of the seismic design in the L'Aquila earthquake in 2009 [7]. Following the analysis, recommendations were made for the type of single-story buildings for industrial use, and some possible alternative solutions were proposed to ensure the stability of all architectural specimens. The specific calculations of a typical precast structure were given the magnitude of the forces and/or displacements of the design connections.

In China, Liu et al. [8–10] researched on double-span single-story and double-span two-story prestressed fabricated concrete frames to obtain seismic performance, including rigidity degradation, hysteretic behavior, displacement ductility, and energy dissipation. The results show that the prestressed fabricated concrete frame has a string of good seismic performances and fulfill requirements of *Code for Seismic Design of Buildings*.

As mentioned in the previous paragraph, the authors of this article have studied double-span single-story and double-span two-story prestressed fabricated concrete frames, and these experiments show seismic performance of multispan prestressed fabricated concrete frame. It also shows seismic performance of prestressed fabricated concrete frame with single story and two stories. However, data are still scarce and we need to provide more evidences to further studies. In order to further study mechanical behaviors and ductility characteristics of multistory prestressed fabricated concrete frame structure, this paper investigates single-span three-story prestressed fabricated concrete frame by pseudodynamic test and pseudostatic test focused on seismic performance, such as failure mechanism, rigidity degradation, hysteretic behavior, and curvature ductility.

2. Experimental Program

2.1. Test Setup. The single-span three-story prestressed fabricated concrete frame was named KJ-6. The design of specimens, including size and reinforcement, is summarized in the CAD model shown in Figure 1. The cubic compressive strength which concrete cubes cured on equal condition is $f_{cu} = 45.7\ \text{N/mm}^2$. Single duct of specimen only puts one low relaxation strand, $7\Phi^j15$, which has $f_{py} = 1811\ \text{N/mm}^2$ yield strength and $f_{pt} = 1974\ \text{N/mm}^2$ ultimate strength on the spot survey. $\phi 20$ of HRB335 has $f_{py} = 477\ \text{N/mm}^2$ yield strength practically, employed as common reinforcements. $\phi 6$ of HPB235 has $f_{py} = 294\ \text{N/mm}^2$ yield strength practically, served as stirrups (Table 1).

The experimental specimens were made in factory and then were moved into the laboratory. Firstly, precast components were assembled into an overall framework in field. And then the gaps between beams and columns were sealed by colloid cement of epoxy resin when steel strands have been passed through linear corrugated pipes. Finally, the strands were tensioned at one end with the strain controlled in $\sigma_{con} = 0.75 f_{ptk}$.

Reaction frame for loading was separated with slot to 30 mm gap before experiment, and then, the axial pressure was controlled by two hydraulic jacks on the top of column so that axial compression ratio increases to 0.2. Since the reaction frame was still connected to slot by binder bolt, the gap between them allowed large deformation of frame at the top in the process of lateral force. Besides, the axial pressure remains the same during the whole experimental stage.

The MTS servohydraulic test systems afforded lateral force to frame using three electrohydraulic servo actuators. The direction of actuator pushing the frame is defined as forward loading; otherwise, it is defined as reverse loading. The maximum thrust of the actuator is 1060 kN, the maximum tension is 670 kN, and the distance is plus or minus 250 mm. Test machines and survey marks are shown in Figure 2. The pseudodynamic testing was carried out by the MTS servohydraulic test systems and the pseudodynamic testware TUT developed by Tsinghua University [11], including α-methods [12, 13] and PC-Newmark methods [14].

The seismic wave is based on the EI-Centro wave, 1940NS, whose waveform figure is shown in Figure 3; the first 10 s were analyzed, and output for time step set up to 0.02 s was obtained. By adjusting the peak ground acceleration to obtain results, peak ground acceleration contains 2×34 gal, 3×34 gal, and 6×34 gal. The pseudostatic testing is accomplished through the MTS servohydraulic test

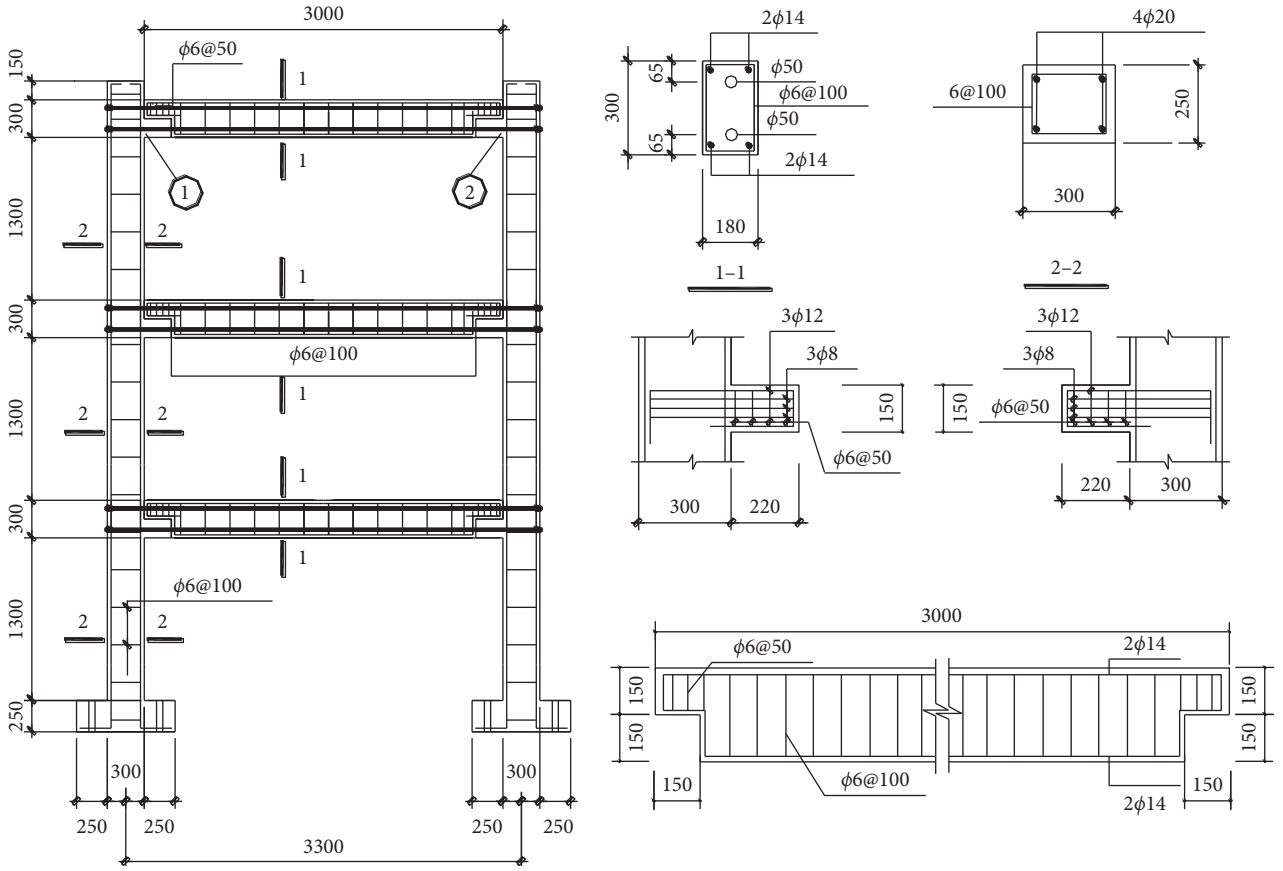

Figure 1: Details of prestressed fabricated concrete frame KJ-6.

Table 1: Mechanical properties of steel bars and prestressed tendons.

Rebar type	Diameter (mm)	Steel grade	Yield strength (MPa)	Ultimate strength (MPa)	Elastic modulus (MPa)
Steel bars	12.0	HRB335	423	586	2.00×105
	14.0	HRB335	397	535	2.00×105
	20.0	HRB335	493	639	2.00×105
Prestressed tendons	15.2	Strands	1811	1974	1.95×105

Note. 1 mm = 0.03937 in; 1 bar = 0.1 MPa = 14.503 psi.

Figure 2: The seismic testing of the single-span three-story prestressed fabricated concrete frame.

systems, and the load-displacement loading method is adopted which is shown in Figure 4. In the previous stage, lateral force was applied as inverted triangular distribution before the frame yielded. In the last stage, lateral displacement was applied by mode of vibration whose lateral displacement ratio is 1.00 : 0.75 : 0.40.

2.2. Loading Procedures of Pseudodynamic Test. The pseudodynamic testing was carried out after the parameters were entered into the computer. When the peak ground acceleration was 2×34 gal, resilience curve changes linear basically, and the frame stays elastic in this stage.

When the peak ground acceleration was 3×34 gal, the maximum forward displacement and reverse displacement of the first-layer top were 3.32 mm and 3.63 mm. The maximum forward displacement and reverse displacement

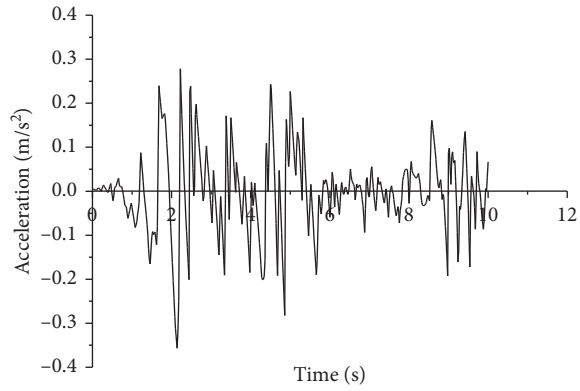

Figure 3: EI-Centro (NS) earthquake wave.

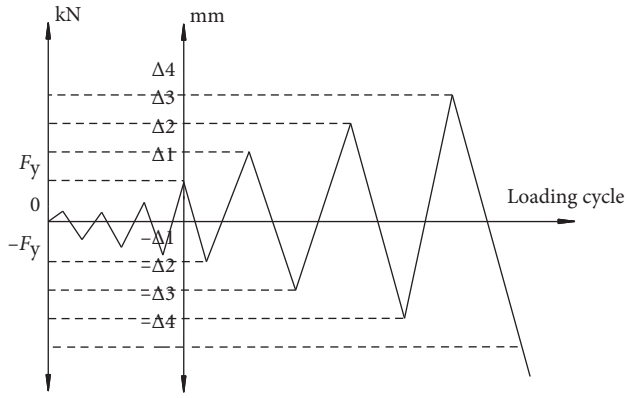

Figure 4: Load-displacement loading method.

of the second-layer top were 6.35 mm and 7.11 mm. The maximum forward displacement and reverse displacement of the third-layer top were 8.86 mm and 10.97 mm. In vertical load, the ends of the beam were influenced by negative bending moment. The forward lateral load made the left end of the beam to be acted on by positive bending moment and cancelled out with the negative bending moment caused by vertical load; the negative bending moments under vertical load and the forward lateral load were superimposed at the right end of the beam, and the cracks grew to 0.1 mm~0.2 mm in the top. Microcracks on the bottom of column were completely closed, and the frame deformation was basically restored when unloading.

When the peak ground acceleration was 6×34 gal, the displacement of three layers suddenly increased, and the maximum forward displacement and reverse displacement of the first-layer top were 9.56 mm and 10.62 mm; the maximum forward displacement and reverse displacement of the second-layer top were 20.21 mm and 22.31 mm; and the maximum forward displacement and reverse displacement of the third-layer top were 25.13 mm and 33.12 mm. Under the superimposition of negative bending moments, the cracks ranging from 0.2 mm to 0.4 mm were appeared in the top of the splicing, and prestressed tendons almost yield. In the compressive zone at the bottom of beam end, the corbel and beam had the horizontal or inclined cracks. Owing to the effect of prestressed tendons after unloading, the deformation of beams can be restored. The deformation of the column cannot be fully recovered, and the frame began to show the plasticity.

2.3. Loading Procedures of Pseudostatic Test. Load-displacement curve matched linear trend, and the frame worked in elastic stage when the lateral force increased to 55 percent of the ultimate load. When the lateral force had been 65 percent of the ultimate loads, low-slope inclined microcracks were appeared in the splicing of corbel and beam, and the microcracks cannot be closed completely. As the load continues to increase, the above cracks extended further. Although spreading slightly in the tensile zone of beam ends and column, the cracks can still close when unloading. Raising the lateral force to 80 percent of the ultimate, the top lateral displacement arrived to 40 mm, the compression concrete area of beam ends has been employed in ultimate state, and the reinforcements yielded in tensile area. There were tiny slant cracks at the bottom of columns, and at that time, lateral displacement loading pattern was adopted. However, the lateral force still increased with the enlargement of displacement.

When the top displacement was up to around 55 mm, the first-layer concrete of corbels on the compression zone began to drop out, and the second-layer beam on the compression zone began to crack mildly and obliquely. When the top displacement was almost 60 mm, several inclined cracks, whose widths were between 0.3 mm and 0.5 mm, were generated at the bottom of the first-layer column, and the lateral force has started to descend. When the top displacement arrived to 95 mm, in the compression zone of beam ends, the first-layer concrete has crushed, and the second-layer concrete began to spall because the strain has reached the ultimate and the third-layer concrete cracked and was slightly damaged. Moreover, the widest decussate crack reached 1.0 mm at the bottom of first-layer column, and the reduction of load-carrying capability was some less obvious.

3. Results

3.1. Results of Pseudodynamic Test. This section shows the results from the dynamic load analysis of the single-span three-story prestressed fabricated concrete frame above.

Figure 5 shows the displacement time-history curves of the frame under different peak ground accelerations. Similarly, Figure 6 shows the restoring force time-history curves under different peak ground accelerations.

The restoring force characteristic curves under different peak ground accelerations are shown in Figure 7. The restoring force characteristic curves, also called hysteretic curve, usually possess hysteretic properties and loop shape, reflecting the mechanical properties well such as strength, stiffness, ductility, and energy dissipation. During the experiment, three electrohydraulic servo actuators applied random seismic wave to each layer of the frame, but the displacement of each layer could not be synchronized

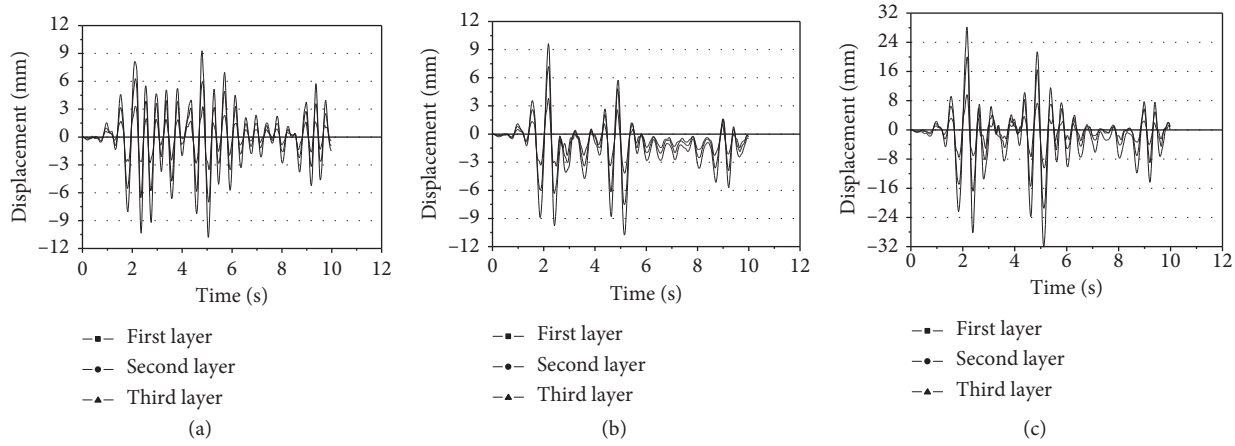

Figure 5: Displacement time-history curves of the prestressed fabricated concrete frame. (a) PGA = 2 × 34 gal. (b) PGA = 3 × 34 gal. (c) PGA = 6 × 34 gal.

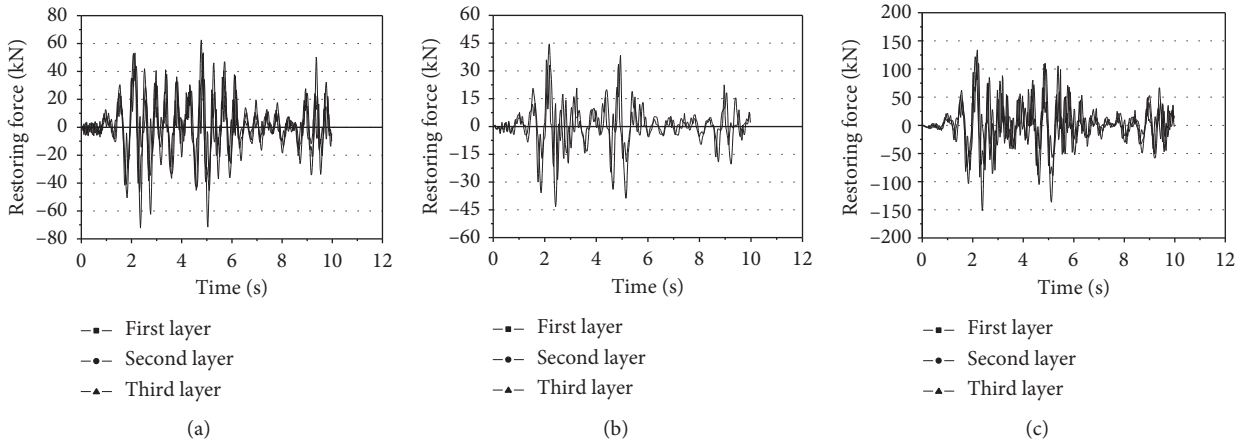

Figure 6: Restoring force time-history curves of the prestressed fabricated concrete frame. (a) PGA = 2 × 34 gal. (b) PGA = 3 × 34 gal. (c) PGA = 6 × 34 gal.

because of other layer constraints. The third-layer restoring force characteristic curve is linearly distributed under 2 × 34 gal, and the structure performed well in energy consumption, as the frame was in the elastic state. The third-layer restoring force characteristic curve shows pinch phenomenon under 6 × 34 gal, and the frame was in the certain plastic state, while energy consumption did not significantly change. Compared with the first-layer restoring force characteristic curve under 2 × 34 gal, the restoring force characteristic curve at 6 × 34 gal is more full, and more energy was consumed. Moreover, the frame showed a plastic state, and the deformation recovered well under the action of prestressed tendons.

Table 2 shows the interlayer drift and drift ratio of the frame under different peak ground accelerations. The maximum interlayer drift ratio is 0.27% under 2 × 34 gal and 3 × 34 gal. The maximum drift ratio between layers is 0.73% under 6 × 34 gal, which is obviously larger than the previous two conditions, indicating that the structure has presented plasticity. The results show that the frame can meet the requirement of the three-level design in China.

According to the results of the pseudodynamic test, the curves of peak ground accelerations-interlayer maximum displacements were obtained (Figure 8). Under 2 × 34 gal and 3 × 34 gal, the maximum displacement of layer is almost a straight line. The maximum displacement of each layer is abruptly changed under 6 × 34 gal, which was significantly larger than the previous two conditions. With the increase of floors, the rising speed was faster, indicating that the frame had shown plasticity.

During the testing process, the displacement and interlayer shear force are obtained, and the interlayer shear force is divided by the interlayer displacement, which is the cross-sectional stiffness of the frame layer, and the peak acceleration and the interlayer stiffness relation curve can be obtained.

Interlayer shear force divided by interlayer displacement, that is, interlayer secant stiffness. The relationship of peak ground acceleration and interlayer stiffness is shown in Figure 9. As the peak ground acceleration of input value increased, the cracking and damages were gradually revealed, and the interlayer stiffness deteriorated gradually.

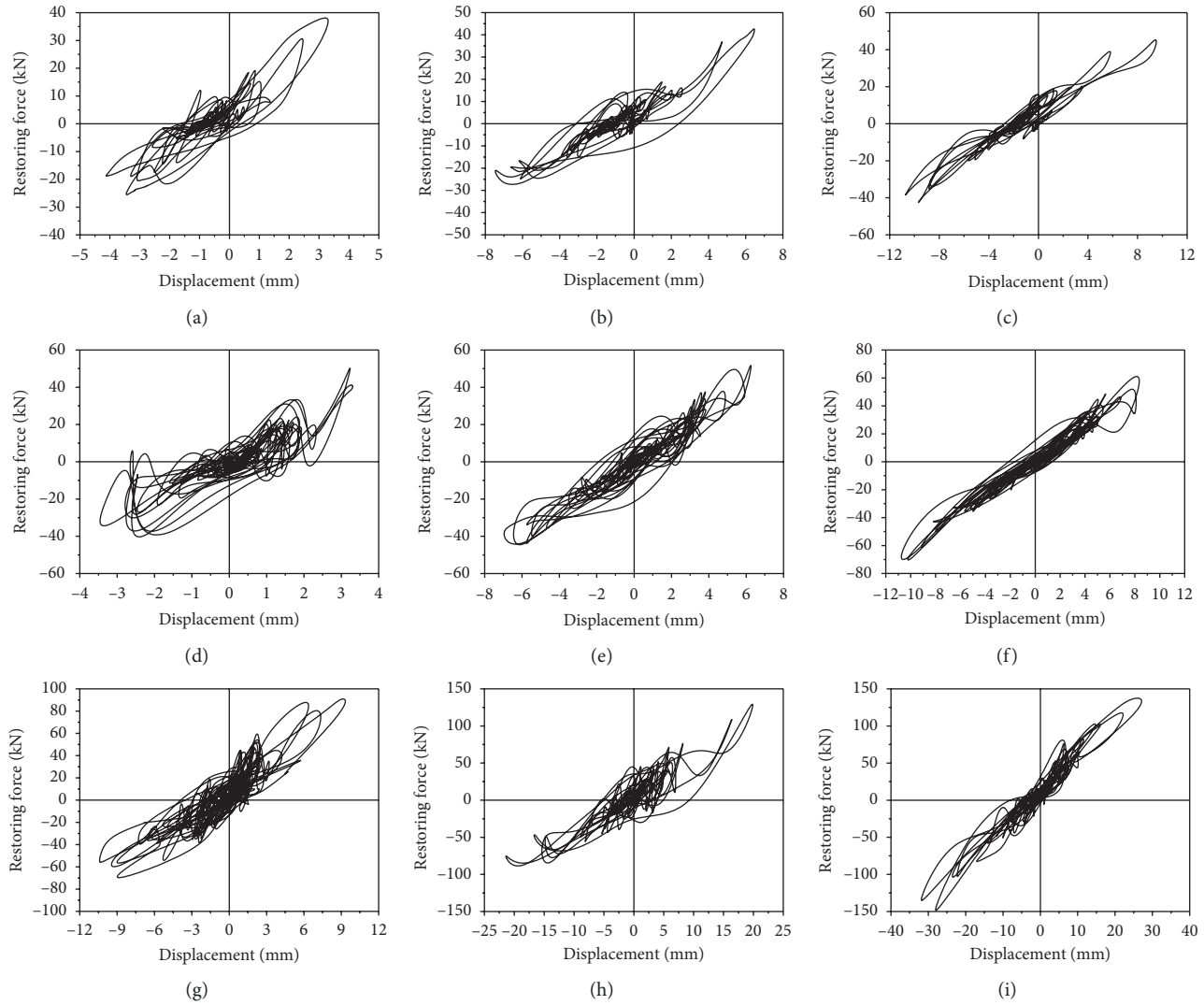

Figure 7: Restoring force characteristic curves of the prestressed fabricated concrete frame. (a) PGA = 2 × 34 gal (first layer). (b) PGA = 2 × 34 gal (second layer). (c) PGA = 2 × 34 gal (third layer). (d) PGA = 3 × 34 gal (first layer). (e) PGA = 3 × 34 gal (second layer). (f) PGA = 3 × 34 gal (third layer). (g) PGA = 6 × 34 gal (first layer). (h) PGA = 6 × 34 gal (second layer). (i) PGA = 6 × 34 gal (third layer).

Due to the dissimilar degree of damage in each layer, there was a difference in the stiffness degradation of the interlayer stiffness. In the case of the sections and heights of column being the same, the columns are bolted to the test stand, so the bottom layer stiffness is approximately 1.5 times the stiffness of the second layer. Since the top of frame is a free end, the stiffness of third layer is about 0.5 times the stiffness of the second layer.

3.2. Results of Pseudostatic Test. This section shows the results from the low reversed cyclic load analyses of the single-span three-story prestressed fabricated concrete frame above. The experiment demonstrates that the third-layer beam ends did not yield and the others beam ends had formed plastic hinges successively. Finally, because of the yield of reinforcements, the crush of concrete, and the appearance of cracks, the lateral force decreased and the structure failed. The crack resistance of the core area has been substantially improved, due to the frame joints in the condition of biaxial compression. Compared with cast-in-place frame, the prestressed fabricated frame has the similar carrying behavior and the beam does fail before the column.

Figure 10 shows the measured lateral displacement under each increasing load from the load-displacement hysteresis curves. Due to the mutual restriction between each actuator, the load-displacement hysteresis curve of the second layer is slightly disordered.

With the increase of displacement, the curve cannot return to the initial point, and the residual deformation increased. It is because the negative bending moments were superimposed on the beam end under the work of lateral force, which increases the plastic deformation of the pressing region. After unloading, the recovery of rotation caused by the negative bending moments lagged because of vertical load.

According to the residual displacement when unloaded and the maximum displacement when failed, the ratio of

Table 2: Interlayer drift ratio of the prestressed fabricated concrete frame in different cases.

Peak ground acceleration	Number of layer	Loading direction	Interlayer drift (mm)	Interlayer drift ratio (%)
2 × 34 gal	1	Forward	3.31	0.207
		Reverse	4.35	0.272
	2	Forward	3.41	0.213
		Reverse	3.63	0.227
	3	Forward	3.14	0.181
		Reverse	3.44	0.215
3 × 34 gal	1	Forward	3.32	0.207
		Reverse	3.63	0.227
	2	Forward	3.03	0.189
		Reverse	3.48	0.217
	3	Forward	3.12	0.195
		Reverse	3.76	0.235
6 × 34 gal	1	Forward	9.56	0.599
		Reverse	10.62	0.662
	2	Forward	10.65	0.667
		Reverse	11.69	0.730
	3	Forward	8.29	0.518
		Reverse	10.81	0.676

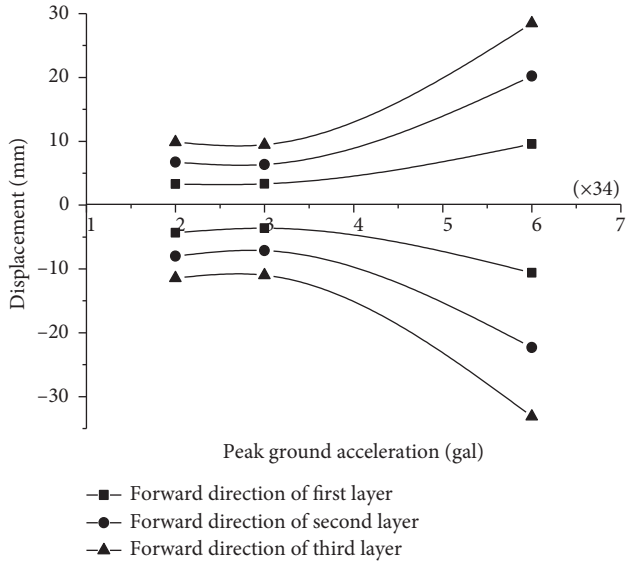

Figure 8: Peak ground accelerations-interlayer maximum displacement curves.

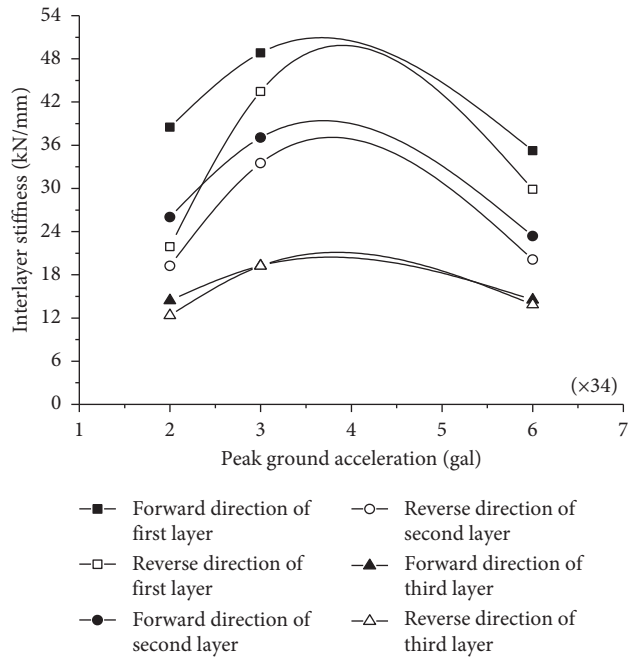

Figure 9: Peak ground acceleration-interlayer stiffness curves.

residual deformation can be calculated, as shown in Table 3. The residual deformation ratio of the first layer is between 0.199 and 0.253; the residual deformation ratio of the second layer is between 0.249 and 0.291; the residual deformation ratio of the third layer is between 0.138 and 0.307. There is no much difference in recovery capability at each layer, and the deformation when loading arrived to the ultimate can still partially recover on account of the prestressing.

The skeleton curves of each layer are shown in Figure 11. The skeleton curve qualitatively compares and measures the seismic performance of specimens. Before cracking, the skeleton curve is oblique lines, indicating that the deformation is elastic. After cracking, the skeleton curve starts to inflect until yield. Meanwhile, the rate constantly decreases and the skeleton curve reaches a turning point, after which the stiffness continually reduces. When reaching about 20 mm, the interlayer displacement continues to increase and the load begins to decrease. The final failure load is approximately 80% to 90% of the peak.

As the loading displacement increases, the cumulative damage will cause the stiffness to gradually decrease with the cycle time. In order to quantitatively reflect the stiffness degradation degree of each loading cycle, the secant stiffness at each loading level is defined as follows:

$$K_j = \frac{\sum_{i=1}^{n} \left| V_j^i \right|}{\sum_{i=1}^{n} \left| \Delta_j^i \right|}, \quad (1)$$

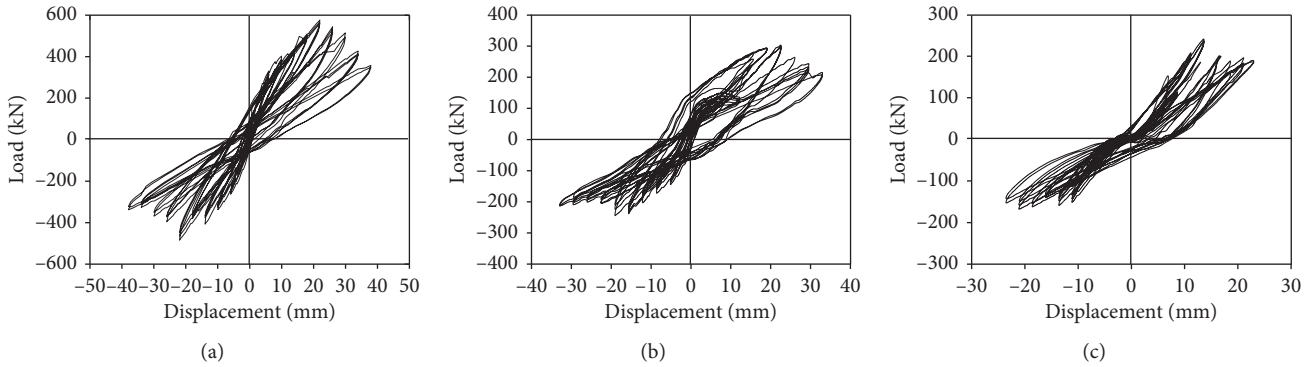

Figure 10: Load-displacement hysteresis curves under low reversed cyclic loading. (a) First layer. (b) Second layer. (c) Third layer.

Table 3: Interlayer drift and energy dissipation of the prestressed fabricated concrete frame.

	Load direction	Yield drift (mm)	Ultimate drift (mm)	Residual drift (mm)	Residual drift ratio	Interlayer yield drift (mm)	Interlayer yield drift ratio (%)	Interlayer ultimate drift (mm)	Interlayer ultimate drift ratio (%)	Equivalent viscous damping coefficient h_e
First layer	Forward	14.7	29	5.0	0.172	14.7	0.917	29	1.818	0.093
	Reverse	15.1	29	8.3	0.286	15.1	0.943	29	1.818	
Second layer	Forward	15.3	70	23.6	0.337	0.6	0.375	41	2.564	0.075
	Reverse	15.9	70	16.2	0.231	0.8	0.500	41	2.564	
Third layer	Forward	43.1	95	30.5	0.321	27.8	1.724	25	1.563	0.070
	Reverse	41.2	95	21.6	0.227	25.3	1.587	25	1.563	

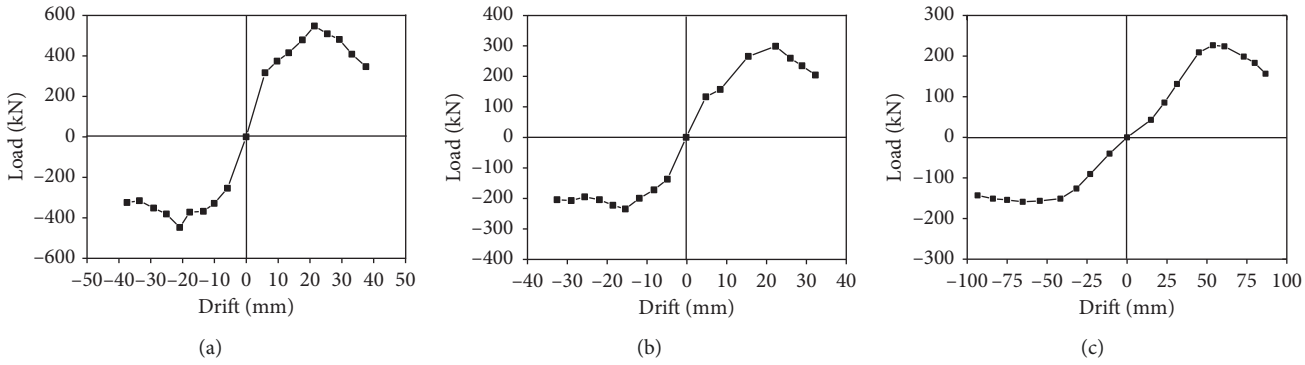

Figure 11: The skeleton curves of each layer. (a) First layer. (b) Second layer. (c) Third layer.

where K_j is the stiffness under the j-th load, V_j^i is the interlayer shear under the j-th load i-th cycle, and Δ_j^i is the interlayer displacement under the j-th load i-th cycle.

In Figure 12, stiffness decreases as the displacement increases. In the previous loading cycles, the stiffness degradation was not obvious; when the cracks were generated, the stiffness degradation increased; entering the yielding phase, the effective section height of the beam continued to decrease, and the stiffness degradation speeded up.

Energy dissipation capacity is an important index to measure the seismic performance of structures. The energy dissipation capacity of structure can be evaluated by the area under the load-displacement hysteresis curve. The envelopes of hysteresis curves in Figure 13 are arched, so the energy dissipation capacity is well.

In addition, the energy dissipation capacity also expressed as equivalent viscous damping coefficient h_e, which is calculated according to the formula in each cycle. After the frame cracked, h_e showed a decrease in each loading cycle. After the frame yielded, h_e kept increasing. The equivalent viscous damping coefficients in the last loading cycle are shown in Table 3, and h_e was between 0.065 and 0.087 when the frame damaged (Figure 14).

$$h_e = \frac{1}{2\pi} \frac{S_{(ABC+CDA)}}{S_{(OBE+ODF)}}. \quad (2)$$

4. Conclusions

This paper investigates the seismic behavior of single-span three-story prestressed fabricated concrete frame, based on pseudostatic testing and pseudodynamic testing such as dynamic characteristics, carrying capacity, hysteresis

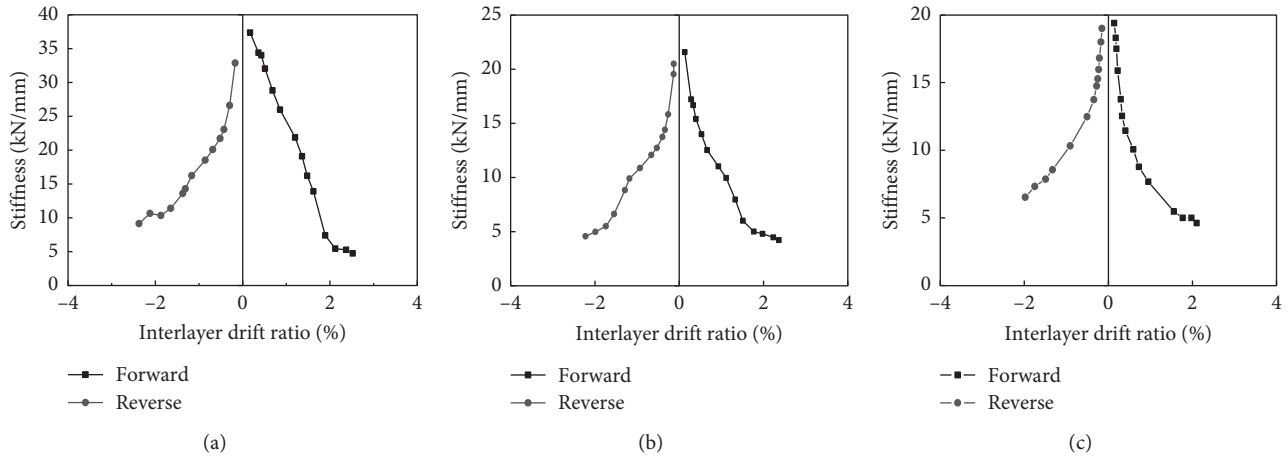

Figure 12: Stiffness degradation curves of the prestressed fabricated concrete frame. (a) First layer. (b) Second layer. (c) Third layer.

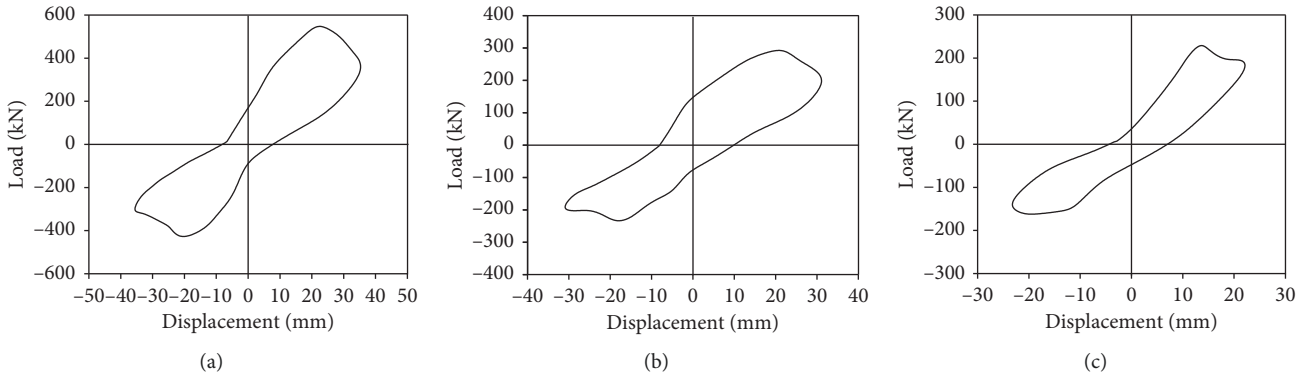

Figure 13: The envelopes of load-displacement hysteresis curves.

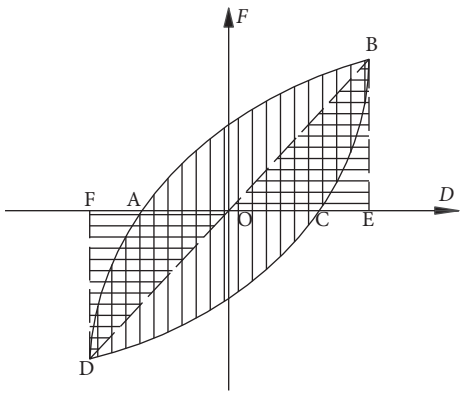

Figure 14: The area graph of load-displacement hysteresis curves.

performance, and energy dissipation. The conclusions of this study are summarized as follows.

(1) In the pseudodynamic test, when the peak ground acceleration was 2×34 gal or 3×34 gal, the displacements had been an inverted triangle. The deformation of frame was able to restore completely after unloading when the maximum interlayer drift ratio arrives 0.27%, and there was no crack appeared in beam and column. When the peak ground acceleration was 6×34 gal, the maximum interlayer drift ratio arrived to 0.73%, and the deformation of beam recovered mainly after unloading. However, the deformation of column recovered incompletely, and the horizontal and oblique cracks had grown in the compressive area of beam bottom showing plasticity.

(2) In the pseudostatic test, the ultimate drift ratio between layers is, respectively, 1.5%, 2.1%, and 2.3% satisfying the limiting value of elastic-plastic drift ratio. In this phase, the beams and columns were damaged slightly and had not been arrived the ultimate condition.

(3) Under the interaction of vertical and horizontal forces, the plastic hinges first appeared at the end of the frame beam where the negative bending moments superimposed. The cracks appeared at the tension zone of beam and splice area of column, and the prestressed strands yielded. Horizontal and oblique cracks appeared at the compression zone of corbel where the concrete crushed. The prestressed fabricated frame achieves the "strong column weak beam" failure mode.

(4) The prestressed fabricated frame has good deformation recovery capability that helps post-earthquake repair and reinforcement. The joint subjected to biaxial compression improved the stiffness and crack resistance of core area, which restricted the deformation of beam and column. Therefore, the prestressed fabricated frame achieves the "strong joints" requirement and the self-centering capacity of the frame enhanced effectively.

Data Availability

The data used to support the findings of this study are available from the corresponding author upon request.

Conflicts of Interest

The authors declare that there are no conflicts of interest regarding the publication of this paper.

Acknowledgments

The authors are grateful for the financial supports received from the National Natural Science Foundation of China (no. 50778060), the National Natural Science Foundation for Young Scientists of China (no. 51608159), and the Specialized Research Fund for the Doctoral Program of Higher Education of China (no. JZ2015HGBZ0509).

References

[1] T. L. Bruce and M. R. Eatherton, "Behavior of post-tensioning strand systems subjected to inelastic cyclic loading," *Journal of Structural Engineering*, vol. 142, no. 10, article 04016067, 2016.

[2] E. Musselman, M. Fournier, P. McAlpine, and S. Sritharan, "Behavior of unbonded post-tensioning monostrand anchorage systems under short duration, high amplitude cyclical loading," *Engineering Structures*, vol. 104, pp. 116–125, 2015.

[3] S. D. Nakaki, "An overview of the PRESSS five-story precast test building," *PCI Journal*, vol. 44, no. 2, pp. 26–39, 1999.

[4] M. N. Priestley, S. Sritharan, J. R. Conley, and S. Pampanin, "Preliminary results and conclusions from the PRESSS five-story precast concrete test building," *PCI Journal*, vol. 44, no. 6, pp. 42–67, 1999.

[5] S. Aaleti and S. Sritharan, "A simplified analysis method for characterizing unbonded post-tensioned precast wall systems," *Engineering Structures*, vol. 31, no. 12, pp. 2966–2975, 2009.

[6] H. Sucuoglu, "Effect of connection rigidity on seismic response of precast concrete frames," *PCI Journal*, vol. 40, no. 1, pp. 94–103, 1995.

[7] G. Toniolo and A. Colombo, "Precast concrete structures: the lessons learned from the L'Aquila earthquake," *Structural Concrete*, vol. 13, no. 2, pp. 73–83, 2012.

[8] B. Liu, Y. Zhang, Z. Jin, F. Shi, and X. Chang, "Experimental study on seismic behavior of prestressed fabricated PC frame connections," *Journal of Building Structures*, vol. 2, p. 010, 2005, in Chinese.

[9] B. Liu, J. Tian, Y. Zhang, Y. Xu, and X. Chang, "Behavior of ductility and energy dissipation of prestressed precast concrete frame under low-cyclic reversed loading," *Journal of Building Structures*, vol. 3, p. 009, 2007, in Chinese.

[10] B. Liu, M. Song, Y. Jiang, S. Huang, and A. Zhou, "Experimental study on seismic performance of post-tensioned precast prestressed concrete frame," *Journal of Building Structures*, vol. 32, pp. 24–32, 2011, in Chinese.

[11] F. Qiu, P. Pan, J. Qian, and Y. Song, "Development and application of pseudodynamic testing software," *Journal of Building Structures*, vol. 21, pp. 22–32, 2000, in Chinese.

[12] P. S. B. Shing, M. T. Vannan, and E. Cater, "Implicit time integration for pseudodynamic tests," *Earthquake Engineering & Structural Dynamics*, vol. 20, no. 6, pp. 551–576, 1991.

[13] O. S. Bursi and P. S. Shing, "Evaluation of some implicit time-stepping algorithms for pseudodynamic tests," *Earthquake Engineering & Structural Dynamics*, vol. 25, no. 4, pp. 333–355, 1996.

[14] M. Nakashima and H. Takai, *Use of Substructure Techniques in Pseudo Dynamic Testing*, Building Research Institute Ministry of Construction, Tsukuba, Japan, 1985.